nature physics

ARTICLES

https://doi.org/10.1038/s41567-020-01040-y

Check for updates

Inertial spin dynamics in ferromagnets

Kumar Neeraj[1,12], Nilesh Awari[2,12], Sergey Kovalev[2], Debanjan Polley[1], Nanna Zhou Hagström[1], Sri Sai Phani Kanth Arekapudi[3], Anna Semisalova[4,5], Kilian Lenz[5], Bertram Green[2], Jan-Christoph Deinert[2], Igor Ilyakov[2], Min Chen[2], Mohammed Bawatna[2], Valentino Scalera[6], Massimiliano d'Aquino[7], Claudio Serpico[6], Olav Hellwig[3,5], Jean-Eric Wegrowe[8], Michael Gensch[9,10] and Stefano Bonetti[1,11]✉

The understanding of how spins move and can be manipulated at pico- and femtosecond timescales has implications for ultrafast and energy-efficient data-processing and storage applications. However, the possibility of realizing commercial technologies based on ultrafast spin dynamics has been hampered by our limited knowledge of the physics behind processes on this timescale. Recently, it has been suggested that inertial effects should be considered in the full description of the spin dynamics at these ultrafast timescales, but a clear observation of such effects in ferromagnets is still lacking. Here, we report direct experimental evidence of intrinsic inertial spin dynamics in ferromagnetic thin films in the form of a nutation of the magnetization at a frequency of ~0.5 THz. This allows us to reveal that the angular momentum relaxation time in ferromagnets is on the order of 10 ps.

The vast majority of digital information worldwide is stored in the form of tiny magnetic bits in thin-film materials in the hard-disk drives installed in large-scale data centres. The positions of the north and south magnetic poles with respect to the thin-film plane encodes the logical 'ones' and 'zeros', which are written using strongly localized, intense magnetic fields. The dynamics of the magnetization in the writing process is described by the Landau–Lifshitz–Gilbert (LLG) equation, which correctly models the reversal of a magnetic bit at nanosecond timescales. Until 20 years ago, it was believed that all of the relevant physics of magnetization dynamics was included in this equation and that optimization of storage devices could be based solely on it.

However, the pioneering experiment of Bigot et al. in 1996[1] revealed the occurrence of spin dynamics on subpicosecond scales that could not be described by the LLG equation, giving birth to the field of ultrafast magnetism. This field explores some of the currently most investigated and debated topics in condensed matter physics[2–20], with implications for both our fundamental understanding of magnetism as well as possible applications for faster and more energy-efficient data manipulation[21]. Recently, the LLG equation was reformulated to include a term to obtain a physically correct inertial response, which was not present in the original formulation[22–32]. This term predicts the appearance of spin nutations, similar to the ones of a spinning top, at a frequency much higher (in the terahertz range) than the spin precession described by the conventional LLG equation (typically at gigahertz frequencies). However, the lack of intense magnetic field sources at these high frequencies has hampered the experimental observation of such nutation dynamics.

In this work, we use intense narrowband terahertz magnetic field transients from a superradiant terahertz source and the femtosecond magneto-optical Kerr effect (MOKE) to detect inertial magnetization effects in ferromagnetic thin films. We find evidence for nutation dynamics with a characteristic frequency of the order of 1 THz, which is damped on timescales of the order of 10 ps. We are able to qualitatively describe the observed magnetization dynamics with a macrospin approximation of the inertial LLG equation and highlight implications for ultrafast magnetism, and magnetic data processing and storage.

According to the LLG equation, the dynamics of the magnetization $\mathbf{M}$ in a ferromagnetic sample are described as[33]

$$\frac{\mathrm{d}\mathbf{M}}{\mathrm{d}t} = -|\gamma|\mathbf{M}\times\left(\mathbf{H}_{\mathrm{eff}} - \frac{\alpha}{|\gamma|M_{\mathrm{s}}}\frac{\mathrm{d}\mathbf{M}}{\mathrm{d}t}\right) \quad (1)$$

where $|\gamma|/2\pi \approx 28\,\mathrm{GHz\,T^{-1}}$ is the gyromagnetic ratio, $\mathbf{H}_{\mathrm{eff}}$ is the effective magnetic field, calculated as the variational derivative of energy with respect to the magnetization, M_{s} is the saturation magnetization and α is the so-called Gilbert damping. The first term on the right-hand side describes the precession $\mathbf{M}$ of a ferromagnetic system around $\mathbf{H}_{\mathrm{eff}}$, while the second term is the damping term, which relaxes the system to an equilibrium state where $\mathbf{M}$ and $\mathbf{H}_{\mathrm{eff}}$ are parallel and no torque is exerted on the magnetization. Figure 1a illustrates schematically the magnetization precession around the effective magnetic field. A resonance peak of the precession can be seen in the frequency domain and it corresponds to the so-called ferromagnetic resonance (FMR). Here, the motion of the spin system is treated as analogous to a classical spinning top. Hence, one can derive the equation of motion of spins in a magnetic field similar to that of a spinning top in a gravitational field. Along similar lines, Gilbert introduced a Lagrangian for the ferromagnetic systems with

[1]Department of Physics, Stockholm University, Stockholm, Sweden. [2]Institute of Radiation Physics, Helmholtz-Zentrum Dresden-Rossendorf, Dresden, Germany. [3]Institute of Physics, Chemnitz University of Technology, Chemnitz, Germany. [4]Faculty of Physics and CENIDE, University of Duisburg-Essen, Duisburg, Germany. [5]Institute of Ion Beam Physics and Materials Research, Helmholtz-Zentrum Dresden-Rossendorf, Dresden, Germany. [6]DIETI, University of Naples Federico II, Naples, Italy. [7]Department of Engineering, University of Naples 'Parthenope', Naples, Italy. [8]LSI, École Polytechnique, CEA/DRF/IRAMIS, CNRS, Institut Polytechnique de Paris, Palaiseau, France. [9]Institute of Optical Sensor Systems, German Aerospace Center (DLR), Berlin, Germany. [10]Institute of Optics and Atomic Physics, TU Berlin, Berlin, Germany. [11]Department of Molecular Sciences and Nanosystems, Ca' Foscari University of Venice, Venezia-Mestre, Italy. [12]These authors contributed equally: K. Neeraj, N. Awari. ✉e-mail: stefano.bonetti@fysik.su.se

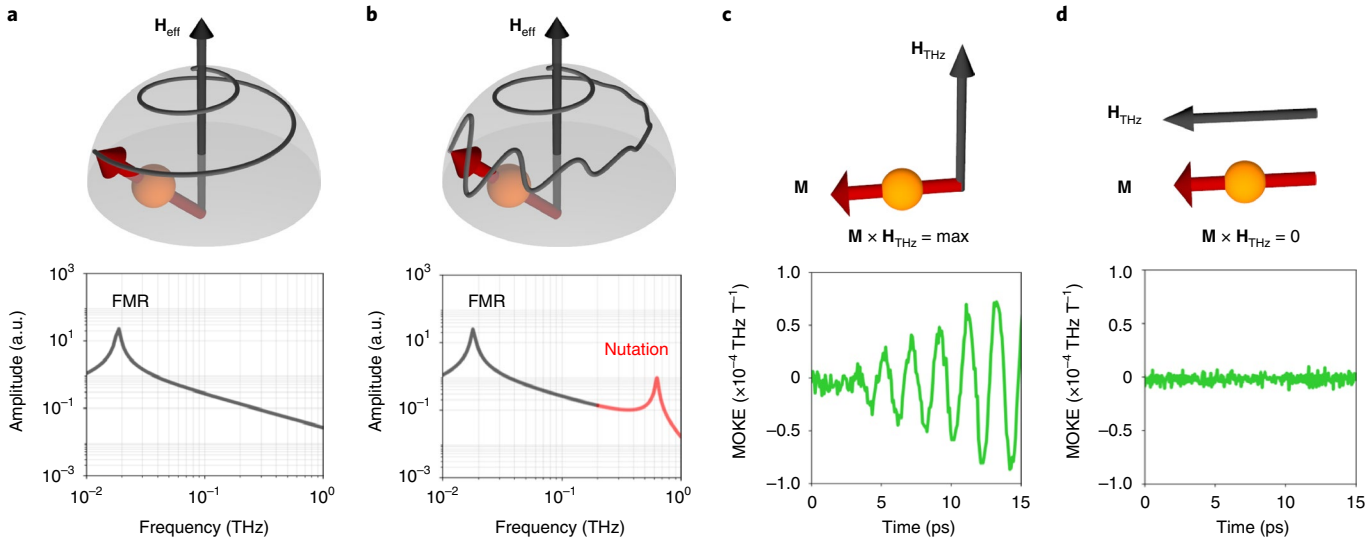

Fig. 1 | Magnetic torque dynamics of a ferromagnet in the terahertz range. a, Top: schematic of the magnetization dynamics and relaxation around an effective magnetic field *H* according to the standard LLG equation. Bottom: LLG-simulated response (that is, the susceptibility) of a ferromagnetic system to an external a.c. magnetic field of varying frequency. **b**, Similar to **a**, but considering the inertial formulation of the LLG equation described in the text. **c**, Top: the geometrical configuration that maximizes the torque of $\mathbf{H}_{THz}$ on the magnetization **M** (that is, when they are orthogonal). Bottom: measured response from the polycrystalline NiFe sample in the maximum torque configuration and with a driving field centred at around 0.6 THz. **d**, Similar to **c** but when $\mathbf{H}_{THz}$ and **M** are parallel; no torque is exerted on the same sample by the same driving field.

an ad hoc inertia tensor. In this mechanical approach for describing the motion of spins, the two principal moments of inertia were set to zero, so that the inertial terms disappear from the dynamic equation. An inertial tensor of this kind is not physically correct[33]; however, despite its crudeness, this approximation turned out to be good enough to describe the dynamics of magnetization on timescales of 0.1 ns or longer, and the general validity of the equation at faster timescales was not questioned.

The concept of mass and inertia in macroscopic systems (such as domain walls) was first introduced by Döring in 1948[34]. In 2004, Zhu et al.[35] showed that the dynamics of spins in a tunnelling barrier between two superconductors has an unusual spin behaviour, in contrast to a simple spin precession, and they termed it a 'Josephson nutation'. Kimel et al.[36] for the first time showed inertia-driven spin switching in antiferromagnetically ordered systems. According to ref. [36], a very short (femtosecond) magnetic impulse can impart enough energy to the spin system to overcome the potential barrier and flip its orientation. In these examples, the inertial terms are due to the non-homogeneity of the magnetic configurations (domain walls, antiferromagnetism, ferrimagnetism and so on), meaning they are due to the presence of the exchange interaction between spins. However, the concept of intrinsic inertia for homogeneous magnetic configurations (typically for a single magnetic dipole or a single spin) arrived only later[22,24–31], and led to the so-called inertial LLG equation:

$$\frac{\mathrm{d}\mathbf{M}}{\mathrm{d}t} = -|\gamma|\mathbf{M}\times\left[\mathbf{H}_{\mathrm{eff}} - \frac{\alpha}{|\gamma|M_{\mathrm{s}}}\left(\frac{\mathrm{d}\mathbf{M}}{\mathrm{d}t} + \tau\frac{\mathrm{d}^2\mathbf{M}}{\mathrm{d}t^2}\right)\right] \qquad (2)$$

The last term of equation (2) has a second derivative term (due to angular momentum relaxation), in addition to the spin precession and damping. This term comes into the picture if one considers the moment of inertia while solving the Landau–Lifshitz (LL) equation based on the classical analogue of a spinning top[22,37]. Simulations reveal that, on timescales shorter than the angular momentum relaxation time τ, nutation oscillations are present on top of the precession motion, as shown in Fig. 1b, identifying a novel 'nutation regime' driven by intrinsic inertia that has yet to be observed experimentally. On timescales longer than τ, the usual LLG equation is recovered. The possible large separation between the timescales of the two regimes would then explain the success of the standard LLG equation in correctly describing magnetization dynamics for times larger than τ. The determination of the value of τ is, however, an open problem that needs to be addressed experimentally, as different theoretical studies indicate values ranging from a few femtoseconds to hundreds of picoseconds[22,30,32,34,37].

To attack this problem, one needs to be able to perform magnetic field spectroscopy in the terahertz range, a task that was technically unfeasible until very recently, when intense terahertz sources started to become available. In the past few years, broadband terahertz radiation generated with table-top laser sources[38] has been exploited to study magnetization dynamics in different classes of material[39–44]. In addition to demagnetization effects similar to those observed with near-infrared radiation, the terahertz magnetic field $\mathbf{H}_{THz}$ of this intense radiation can exert a Zeeman torque $\mathbf{M}\times\mathbf{H}_{THz}$, leading to a coherent precessional motion of the magnetization vector **M** that lasts until the terahertz pulse has left the material. Those table-top sources, while having the necessary terahertz bandwidth to perform the proposed magnetic field spectroscopy, are not spectrally dense, and the detection of a nutation resonance driven by inertia has not been reported yet.

However, intense and tunable narrowband terahertz magnetic fields can now be generated at superradiant electron sources such as the TELBE facility in Dresden, Germany[45,46]. Here, we used the radiation generated at TELBE to drive the magnetization of thin-film ferromagnets with a strong periodic terahertz magnetic field. The basic idea is to perform a forced oscillator experiment as a function of the frequency of the terahertz magnetic field $\mathbf{H}_{THz}$, detecting the amplitude and phase of the response with the femtosecond MOKE in an attempt to observe the signature of a resonance. The response of the magnetization is maximized when $\mathbf{H}_{THz}$ and the static magnetization (which is controlled with an external magnetic field) are orthogonal to each other. This is illustrated schematically in the top panels of Fig. 1c,d, with the corresponding experimental measurement in the bottom panels, where we show the detected polar MOKE signal. That the terahertz-driven dynamics in thin magnetic

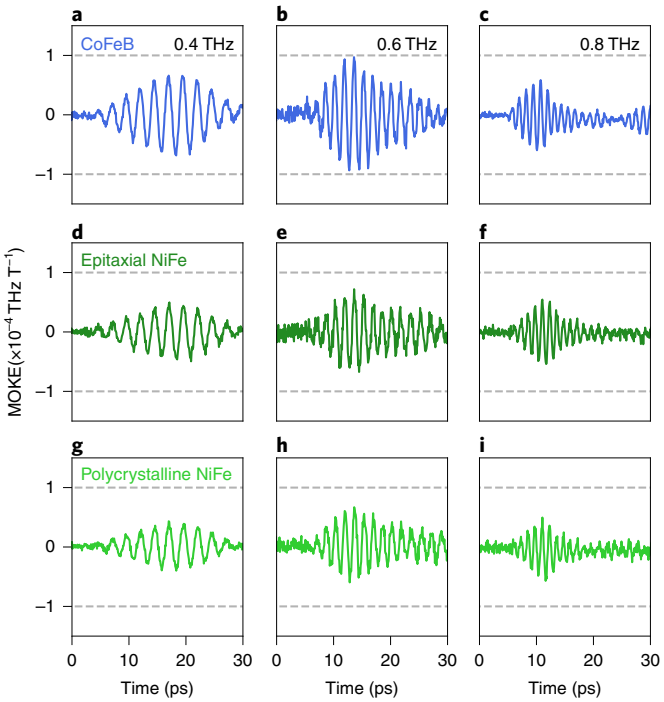

Fig. 2 | Coherent MOKE response of different thin-film ferromagnets. **a**–**i**, Time-resolved MOKE response of the magnetization to narrowband terahertz fields centred around 0.4 (**a**,**d**,**g**), 0.6 (**b**,**e**,**h**) and 0.8 THz (**c**,**f**,**i**) for an amorphous CoFeB film on silicon (**a**–**c**), an epitaxial $Ni_{81}Fe_{19}$ (permalloy) film grown on a MgO (100) substrate (**d**–**f**) and polycrystalline $Ni_{81}Fe_{19}$ deposited on a MgO (111) substrate (**g**–**i**). The data are normalized according to equation (3) and related considerations in the main text.

films is a genuine magnetic effect and not an optical artefact has now been shown in several works. In ref. [47] it was shown that the response of a similar magnetic film, when either the externally applied magnetic field or the terahertz magnetic field polarity is reversed, has the symmetry expected of a magnetic effect. The polar MOKE configuration is the optimal geometry because the torque acts out of the film plane when both $\mathbf{H}_{\mathrm{THz}}$ and $\mathbf{M}$ are in the plane. Further details of the experimental set-up are given in the Methods and in Supplementary Sections 1–3. However, we comment here on the normalization procedure, which is a key aspect when measuring absolute amplitudes. With the realistic assumptions that the first term on the right-hand side of equations (1) and (2) is much larger than the other terms, and that the magnetization responds linearly to the field, one can read the response of the magnetization as the integral of the terahertz magnetic field. Approximating the terahertz magnetic field as a sinusoidal excitation with angular frequency ω, in the case of orthogonal $\mathbf{M}$ and $\mathbf{H}_{\mathrm{THz}}$, the temporal response of the normalized magnetization $m(t) = M(t)/M_s$ ignoring resonance effects can be simplified as

$$m(t) = |\gamma| \int H_{\mathrm{THz}} \sin \omega t \; \mathrm{d}t = |\gamma| \frac{H_{\mathrm{THz}}}{\omega} \cos \omega t \qquad (3)$$

with the magnetization starting to move out of the plane of the film when $\mathbf{M}$ and $\mathbf{H}$ are in the film plane. Hence, to estimate the proper response of the magnetic films to the terahertz magnetic field, the data presented in Figs. 2 and 4 have been normalized by the magnitude H_{THz} and by the frequency ω of the THz pulse.

We investigated three different thin-film samples, all with easy-plane magnetization: amorphous CoFeB grown on a Si/SiO_2 substrate, and epitaxial and polycrystalline permalloy films grown on single-crystal MgO (100) and (111) substrates, respectively. Those samples have different Gilbert damping parameter α and saturation magnetization M_s, which we measured with standard FMR spectroscopy as shown in Supplementary Section 4. Both parameters modulate the magnitude of the additional inertial term introduced in equation (2).

Figure 2 shows the amplitude of the femtosecond MOKE response of the three ferromagnetic thin-film samples after excitation with narrowband terahertz pulses with a centre frequency of 0.4, 0.6 or 0.8 THz. The characterization of the narrowband terahertz pulses, performed with electro-optical sampling, is described in the Methods. The terahertz magnetic field was applied orthogonal to the equilibrium magnetization direction as discussed above, so as to maximize the torque. In all cases, a clear coherent response of the magnetization to the narrowband terahertz field is observed. After the normalization procedure discussed above, the overall response seems to be slightly larger for the CoFeB samples, probably related to the larger magneto-optical response of that sample as compared to permalloy. Hence, to infer real magnetic effects (as compared to magneto-optical ones), absolute amplitudes should be compared only within the same sample at different frequencies, and not between different samples. With this consideration, one can observe an evident change in the amplitude of the response within each sample when the frequency is changed, with the largest effect observed at ~0.5–0.6 THz for all three cases.

The observed response of the magnetization confirms the analogy with a forced oscillator, where the terahertz magnetic field acts as the driving periodic force, to which the magnetization responds, in the linear regime, by integrating it. The modulation of the amplitude of the response suggests already the presence of an underlying resonance at ~0.6 THz superimposed onto the purely off-resonant, forced response of lower amplitude. To further validate this point, in Fig. 3 we analysed the relative phase shift between the integral of the driving force (the terahertz magnetic field, which is reconstructed independently via experimental electro-optical sampling) and the experimental MOKE signal far away from the maximum response (0.4 THz) and close to the maximum response (0.6 THz). We show here data for one of the samples, but similar trends are observed for the other two (Supplementary Section 5). The data show that, at 0.4 THz, the magnetization precession is in phase with the driving field, and this is also reproduced by simulations solving the inertial LLG equation[25,48], including the experimentally measured terahertz magnetic field as the driving force. (See Supplementary Section 6 for details.) At 0.6 THz, on the other hand, the magnetization precession and driving field are ~90° out of phase, which is also reproduced by the simulations. This fact reinforces the statement that an underlying resonance is present in the system, at a frequency two orders of magnitude higher than any known ferromagnetic resonance and which is determined by one single fitting parameter τ, that is, the angular momentum relaxation term in equation (2).

To estimate the value of τ from experiments, we plot in Fig. 4a the amplitude of the measured response at six different frequencies. A fit with a Lorentzian curve was used to return the centre frequency ω_{n}. According to ref. [27], the nutation frequency is

$$\omega_{\mathrm{n}} = \frac{\sqrt{1 + \alpha\tau|\gamma|H}}{\alpha\tau} \approx 1/\alpha\tau \qquad (4)$$

We measured the Gilbert damping α independently with ferromagnetic resonance spectroscopy in all three samples and extracted the corresponding τ, as summarized in Table 1. Numerical calculations that solve the inertial LLG equation with these values of τ are shown in Fig. 4b, and reproduce the main features of the experimental data.

We now make several considerations looking at Fig. 4 and Table 1. The first observation is that the peak centre frequency moves by ~10% between the different materials, almost independently of α.

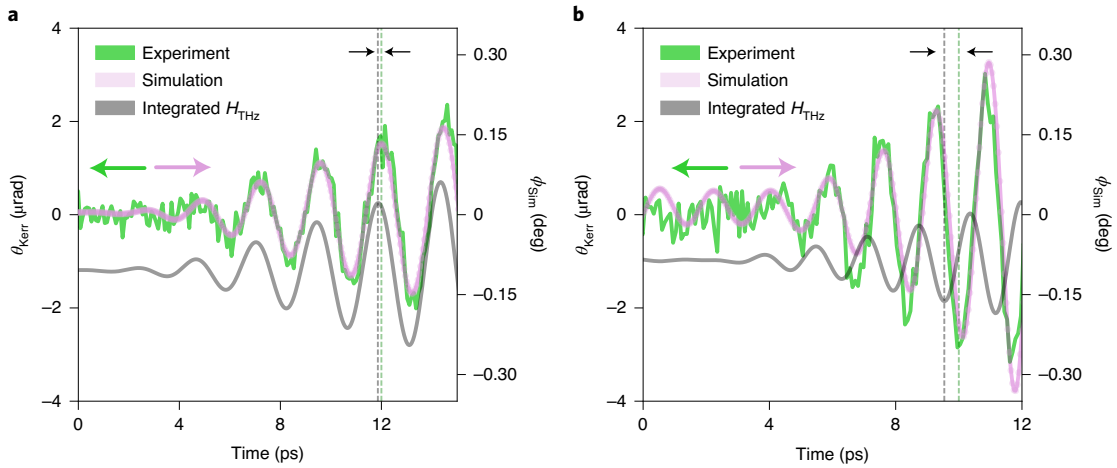

Fig. 3 | Effect of the driving field frequency on the phase of the response of the magnetization. a,**b**, Comparison of the phase-resolved MOKE response at 0.4-THz (**a**) and 0.6-THz (**b**) centre frequency of the terahertz magnetic field pulse for the polycrystalline permalloy film. Green curves: experimentally measured magneto-optical Kerr rotations, without the scaling described by equation (3). The absolute values of rotation for both frequencies are plotted on the left vertical axes. Pink curves: simulated response using the inertial LLG equation with $\tau = 11.3$ ps and using the experimentally measured H_{THz} field amplitude. The right vertical axes show the simulated nutation angle. Grey curves: time integral of the experimental terahertz magnetic field H_{THz}. The vertical dashed lines illustrate the phase difference between the driving terahertz field and the magnetization dynamics.

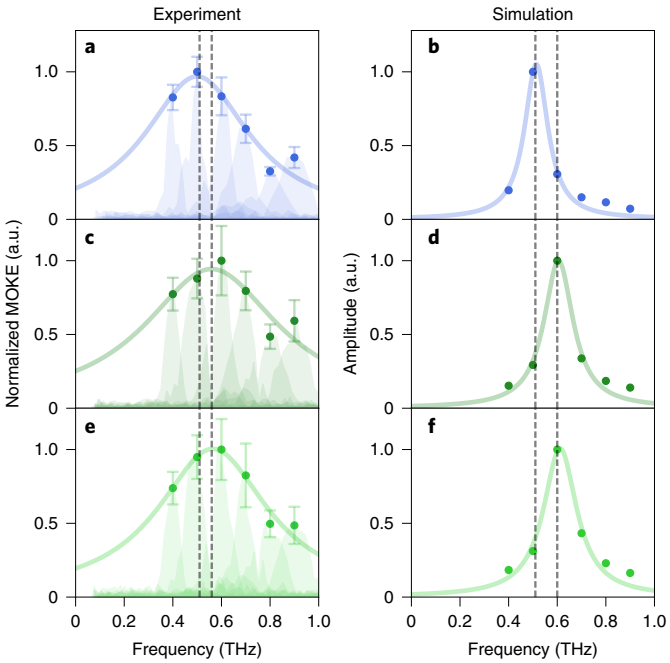

Fig. 4 | Amplitude of the magnetization dynamics for narrowband terahertz fields. a,**c**,**e**, Symbols: experimentally measured maximum of the MOKE amplitude normalized according to equation (3) for CoFeB (**a**), epitaxial NiFe (**c**) and polycrystalline NiFe (**e**), respectively. The shaded curves represent the magnitude of the Fourier transform of the experimental traces at the different centre frequencies. Error bars represent the standard deviation of noise before the arrival of the terahertz pulse, first measured in absolute units and then scaled by the same amplitude with the signal. **b**,**d**,**f**, Calculated maximum magnetization response amplitudes solving the inertial LLG equation, corresponding to **a**, **c** and **e**. Solid lines: Lorentzian fit to the data points.

Interestingly, even though the relative uncertainty is large, the nutation frequency for the two NiFe samples is the same, and slightly different from the one of the CoFeB sample. The nutation frequency ω_n is also very weakly dependent on the applied magnetic field; solving the inertial LLG equation, we estimated that one would need a 10-T applied field to shift the peak by ~200 GHz, which should be detectable even given the large width of the resonance. The measured nutation frequencies are, for all samples, in the range predicted by ref. [32].

A second important observation is that the width of the experimental peak is larger than what simulations predict. This mismatch can potentially be attributed to the fact that the inertial motion of the spins might be affected by the microscopic details of the material. The inertial dynamics has been reported to remain the same if one considers the dynamics of a macroscopic magnetic volume element[29]. However, it is surprising that the different materials with different textures that we investigate here show no appreciable difference in linewidth. We have performed micromagnetic simulations and did not observe substantial linewidth broadening. We have also checked that finite temperature effects, included in the simulations as a random fluctuation of the effective magnetic field acting on the magnetization, did not substantially affect the linewidth. Further considerations are beyond the scope of this work and we leave this question open to future investigations.

Finally, we comment on the experimentally extracted values of τ of the order of 10–100 ps. These are one to two orders of magnitude larger than those obtained with indirect spectroscopy experiments observing the stiffening of the ferromagnetic resonance, but with no phase information[48]. This is a discrepancy that we cannot reconcile at the moment, but we believe that our direct measurement of the resonant nutation frequency, with amplitude and phase information, gives a more accurate estimate of the relaxation time. The extracted τ is also greater than the timescales observed in recent studies looking at the relaxation of the magnetization with phonons[17,19] and magnons[12,18,20]. However, in all these cases, an essential ingredient was the excitation of hot electrons on the order of 1 eV away from the Fermi level by means of femtosecond near-infrared radiation. In this work, the much lower photon energy of the driving terahertz field of the order of 1 meV prevents, by design, the creation of such hot electrons. Hence, a direct comparison between the relaxation timescale of our experiment and the one observed in these studies cannot be made.

An alternative explanation for the presence of a high-frequency magnetic excitation could be the presence of exchange-dominated

Table 1 | Centre frequency ω_n, the full-width at half-maximum (FWHM), the Gilbert damping α and the angular momentum relaxation time τ for the three samples

Sample	Centre frequency $\omega_n/2\pi$ (THz)	FWHM (THz)	α	$\tau=1/\alpha\omega_n$ (ps)
CoFeB	0.50 ± 0.10	0.58	0.0044	72 [−13, +17]
Epitaxial NiFe	0.56 ± 0.12	0.67	0.0058	49 [−9, +13]
Polycrystalline NiFe	0.56 ± 0.11	0.55	0.0230	12 [−2, +3]

The centre frequency ω_n and the full-width at half-maximum (FWHM) were extracted parameters from the Lorentzian fit of the experimental data plotted in Fig. 4 for all three samples. The Gilbert damping α was measured independently. The angular momentum relaxation time τ was calculated using the approximation of equation (4).

standing spin-wave modes across the film thickness, similar to what was observed in ref. [49]. However, we argue that those modes are not relevant here, simply because they cannot be excited in our experiment. In fact, we directly drive the film with electromagnetic radiation whose k-vector is orders of magnitude smaller than the film thickness and far away from such high-k spin waves. Excitation of large-wavenumber spin waves due to ultrafast demagnetization, caused by the terahertz-induced spin currents observed in ref. [41], are also not expected. In metals and at terahertz frequencies, the skin depth is of the order of 0.1–1 µm, again orders of magnitude larger than the thin-film thickness, hence any spin-current-related effects are, to an excellent approximation, uniform in the sample. At present, our data clearly demonstrate the existence of a resonance in the terahertz regime, whose most plausible theoretical explanation is the excitation of intrinsic nutation dynamics in the magnetic system.

We anticipate that our results will allow for a better understanding of the fundamental mechanisms of ultrafast demagnetization and reversal, with implications for the realization of faster and more efficient magnetic data-processing and storage devices.

Online content

Any methods, additional references, Nature Research reporting summaries, source data, extended data, supplementary information, acknowledgements, peer review information; details of author contributions and competing interests; and statements of data and code availability are available at https://doi.org/10.1038/s41567-020-01040-y.

Received: 30 October 2019; Accepted: 17 August 2020;
Published online: 28 September 2020

References

1. Beaurepaire, E., Merle, J.-C., Daunois, A. & Bigot, J.-Y. Ultrafast spin dynamics in ferromagnetic nickel. *Phys. Rev. Lett.* **76**, 4250–4253 (1996).
2. Koopmans, B., Van Kampen, M., Kohlhepp, J. T. & De Jonge, W. J. M. Ultrafast magneto-optics in nickel: magnetism or optics?. *Phys. Rev. Lett.* **85**, 844–847 (2000).
3. Koopmans, B., Van Kampen, M. & De Jonge, W. J. M. Experimental access to femtosecond spin dynamics. *J. Phys. Condens. Matter* **15**, S723–S736 (2003).
4. Koopmans, B., Ruigrok, J. J. M., Dalla Longa, F. & De Jonge, W. J. M. Unifying ultrafast magnetization dynamics. *Phys. Rev. Lett.* **95**, 267207 (2005).
5. Stamm, C. et al. Femtosecond modification of electron localization and transfer of angular momentum in nickel. *Nat. Mater.* **6**, 740–743 (2007).
6. Longa, F. D., Kohlhepp, J. T., De Jonge, W. J. M. & Koopmans, B. Influence of photon angular momentum on ultrafast demagnetization in nickel. *Phys. Rev. B* **75**, 224431 (2007).
7. Carpene, E. et al. Dynamics of electron–magnon interaction and ultrafast demagnetization in thin iron films. *Phys. Rev. B* **78**, 174422 (2008).
8. Koopmans, B. et al. Explaining the paradoxical diversity of ultrafast laser-induced demagnetization. *Nat. Mater.* **9**, 259–265 (2010).
9. Boeglin, C. et al. Distinguishing the ultrafast dynamics of spin and orbital moments in solids. *Nature* **465**, 458–461 (2010).
10. Kirilyuk, A., Kimel, A. V. & Rasing, T. Ultrafast optical manipulation of magnetic order. *Rev. Mod. Phys.* **82**, 2731–2784 (2010).
11. Battiato, M., Carva, K. & Oppeneer, P. M. Superdiffusive spin transport as a mechanism of ultrafast demagnetization. *Phys. Rev. Lett.* **105**, 027203 (2010).
12. Schmidt, A. B. et al. Ultrafast magnon generation in an Fe film on Cu(100). *Phys. Rev. Lett.* **105**, 197401 (2010).
13. Radu, I. et al. Transient ferromagnetic-like state mediating ultrafast reversal of antiferromagnetically coupled spins. *Nature* **472**, 205–208 (2011).
14. Stefan, M. et al. Probing the timescale of the exchange interaction in a ferromagnetic alloy. *Proc. Natl Acad. Sci. USA* **109**, 4792–4797 (2012).
15. Carva, K., Battiato, M., Legut, D. & Oppeneer, P. M. Ab initio theory of electron–phonon mediated ultrafast spin relaxation of laser-excited hot electrons in transition-metal ferromagnets. *Phys. Rev. B* **87**, 184425 (2013).
16. Lambert, C.-H. et al. All-optical control of ferromagnetic thin films and nanostructures. *Science* **345**, 1337–1340 (2014).
17. Henighan, T. et al. Generation mechanism of terahertz coherent acoustic phonons in Fe. *Phys. Rev. B* **93**, 220301 (2016).
18. Eich, S. et al. Band structure evolution during the ultrafast ferromagnetic–paramagnetic phase transition in cobalt. *Sci. Adv.* **3**, e1602094 (2017).
19. Dornes, C. et al. The ultrafast Einstein–de Haas effect. *Nature* **565**, 209–212 (2019).
20. Iacocca, E. et al. Spin-current-mediated rapid magnon localisation and coalescence after ultrafast optical pumping of ferrimagnetic alloys. *Nat. Commun.* **10**, 1756 (2019).
21. Stanciu, C. D. et al. Subpicosecond magnetization reversal across ferrimagnetic compensation points. *Phys. Rev. Lett.* **99**, 217204 (2007).
22. Ciornei, M.-C., Rubí, J. M. & Wegrowe, J.-E. Magnetization dynamics in the inertial regime: nutation predicted at short time scales. *Phys. Rev. B* **83**, 020410 (2011).
23. Böttcher, D., Ernst, A. & Henk, J. Atomistic magnetization dynamics in nanostructures based on first principles calculations: application to Co nanoislands on Cu(111). *J. Phys. Condens. Matter* **23**, 296003 (2011).
24. Wegrowe, J.-E. & Ciornei, M.-C. Magnetization dynamics, gyromagnetic relation and inertial effects. *Am. J. Phys.* **80**, 607–611 (2012).
25. Olive, E., Lansac, Y. & Wegrowe, J.-E. Beyond ferromagnetic resonance: the inertial regime of the magnetization. *Appl. Phys. Lett.* **100**, 192407 (2012).
26. Bhattacharjee, S., Nordström, L. & Fransson, J. Atomistic spin dynamic method with both damping and moment of inertia effects included from first principles. *Phys. Rev. Lett.* **108**, 057204 (2012).
27. Olive, E., Lansac, Y., Meyer, M., Hayoun, M. & Wegrowe, J.-E. Deviation from the Landau–Lifshitz–Gilbert equation in the inertial regime of the magnetization. *J. Appl. Phys.* **117**, 213904 (2015).
28. Thonig, D., Eriksson, O. & Pereiro, M. Magnetic moment of inertia within the torque–torque correlation model. *Sci. Rep.* **7**, 931 (2017).
29. Mondal, R., Berritta, M. & Oppeneer, P. M. Generalisation of Gilbert damping and magnetic inertia parameter as a series of higher-order relativistic terms. *J. Phys. Condens. Matter* **30**, 265801 (2018).
30. Kikuchi, T. & Tatara, G. Spin dynamics with inertia in metallic ferromagnets. *Phys. Rev. B* **92**, 184410 (2015).
31. Fähnle, M. Comparison of theories of fast and ultrafast magnetization dynamics. *J. Magn. Magn. Mater.* **469**, 28–29 (2019).
32. Bastardis, R., Vernay, F. & Kachkachi, H. Magnetization nutation induced by surface effects in nanomagnets. *Phys. Rev. B* **98**, 165444 (2018).
33. Gilbert, T. L. A phenomenological theory of damping in ferromagnetic materials. *IEEE Trans. Magn.* **40**, 3443–3449 (2004).
34. Böttcher, D. & Henk, J. Significance of nutation in magnetization dynamics of nanostructures. *Phys. Rev. B* **86**, 020404 (2012).
35. Zhu, J.-X., Nussinov, Z., Shnirman, A. & Balatsky, A. V. Novel spin dynamics in a Josephson junction. *Phys. Rev. Lett.* **92**, 107001 (2004).
36. Kimel, A. V. et al. Inertia-driven spin switching in antiferromagnets. *Nat. Phys.* **5**, 727–731 (2009).
37. Fähnle, M., Steiauf, D. & Illg, C. Generalized Gilbert equation including inertial damping: derivation from an extended breathing Fermi surface model. *Phys. Rev. B* **84**, 172403 (2011).
38. Hoffmann, M. C. & Fülöp, J. A. Intense ultrashort terahertz pulses: generation and applications. *J. Phys. D* **44**, 083001 (2011).
39. Kampfrath, T., Tanaka, K. & Nelson, K. A. Resonant and nonresonant control over matter and light by intense terahertz transients. *Nat. Photon.* **7**, 680–690 (2013).
40. Vicario, C. et al. Off-resonant magnetization dynamics phase-locked to an intense phase-stable terahertz transient. *Nat. Photon.* **7**, 720–723 (2013).
41. Bonetti, S. et al. THz-driven ultrafast spin-lattice scattering in amorphous metallic ferromagnets. *Phys. Rev. Lett.* **117**, 087205 (2016).
42. Hafez, H. A. et al. Extremely efficient terahertz high-harmonic generation in graphene by hot Dirac fermions. *Nature* **561**, 507–511 (2018).
43. Noe, G. T. et al. Coherent terahertz excitation of magnons to 30 T. In *2018 Conference on Lasers and Electro-Optics (CLEO)* 1–2 (IEEE, 2018).

44. Polley, D. et al. THz-driven demagnetization with perpendicular magnetic anisotropy: towards ultrafast ballistic switching. *J. Phys. D* **51**, 084001 (2018).
45. Kovalev, S. et al. Probing ultra-fast processes with high dynamic range at 4th-generation light sources: arrival time and intensity binning at unprecedented repetition rates. *Struct. Dyn.* **4**, 024301 (2017).
46. Kovalev, S. et al. Selective THz control of magnetic order: new opportunities from superradiant undulator sources. *J. Phys. D* **51**, 114007 (2018).
47. Hudl, M. et al. Nonlinear magnetization dynamics driven by strong terahertz fields. *Phys. Rev. Lett.* **123**, 197204 (2019).
48. Li, Y., Barra, A.-L., Auffret, S., Ebels, U. & Bailey, W. E. Inertial terms to magnetization dynamics in ferromagnetic thin films. *Phys. Rev. B* **92**, 140413 (2015).
49. Razdolski, I. et al. Nanoscale interface confinement of ultrafast spin transfer torque driving non-uniform spin dynamics. *Nat. Commun.* **8**, 15007 (2017).

Methods

Sample details. The epitaxial permalloy ($Ni_{81}Fe_{19}$ at%) films investigated in the study are 15 nm thick and prepared by magnetron sputter deposition using Ar sputter gas at $p_{Ar} = 3.5 \times 10^{-3}$ mbar. At first, single-crystal MgO (100) substrates were pre-annealed at 873 K for 3 h to remove typical inorganic Mg(OH) layers from the surface, then the substrate was cooled to 550 K for d.c.-magnetron sputtering. The epitaxial relation between the substrate and the film (MgO(100) $[100]_{fcc}||Ni_{81}Fe_{19}(100)[100]_{fcc}$, c/a ratio of 0.99) was confirmed by X-ray diffraction (ϕ-scans along the (111) orientation of the MgO crystal and the NiFe film). After the same substrate pre-annealing step as used above (873 K for 3 h), 15-nm-thick polycrystalline $Ni_{81}Fe_{19}$ films were deposited at room temperature on a MgO (111) substrate. In both cases (epitaxial and polycrystalline), an Al cap layer of 1.5 nm was deposited at room temperature to protect the magnetic films from oxidation. The atomic stoichiometry of the $Ni_{81}Fe_{19}$-alloy thin films were determined by Rutherford backscattering spectrometry within the measurement accuracy of ±1 at%.

Amorphous 10-nm-thick $Co_{40}Fe_{40}B_{20}$ films were sputter-deposited at room temperature from a stoichiometric target on a $Si/SiO_2(100\,nm)/Al_2O_3(10\,nm)$ substrate, followed by an Al (1.5 nm) cap layer. Commercial 2-inch stoichiometric alloy targets of $Ni_{81}Fe_{19}$ and $Co_{40}Fe_{40}B_{20}$ (4N material purity) were produced by liquid metallurgy. The deposition rates were pre-calibrated using X-ray reflectivity measurements and, during the sputtering process, the thicknesses of the individual layers were monitored via a quartz crystal. The saturation magnetization M_s was determined from 3 mm × 3 mm sample pieces using a superconducting quantum interference device vibrating sample magnetometer, and we found the values $M_s = 756\,kA\,m^{-1}$ ($\mu_0 M_s = 0.95$ T) for epitaxial permalloy, $M_s = 738\,kA\,m^{-1}$ ($\mu_0 M_s = 0.93$ T) for polycrystalline permalloy and $M_s = 1{,}290\,kA\,m^{-1}$ ($\mu_0 M_s = 1.62$ T) for amorphous CoFeB.

Experimental set-up. The superradiant terahertz pulse source TELBE delivered multicycle electromagnetic pulses at a repetition rate of 100 kHz. The generated terahertz pulses were linearly polarized with a spectral bandwidth of 20% and a centre frequency tunable between 0.3 and 1.2 THz (ref. [46]). In the experiment described here, the terahertz radiation from TELBE was focused onto the sample using gold-coated off-axis parabolic mirrors. The terahertz electric field was measured in the time domain by free-space electro-optical sampling in a 100-µm-thick ZnTe crystal. A 100-fs-duration laser pulse with a central wavelength of 805 nm, from a commercial Ti:sapphire laser system, was used as a probe. The laser was synchronized with the TELBE source, with a typical timing jitter of ~30 fs (FWHM) between the probe laser and the terahertz pulse generated from the undulator[46,50].

In our measurement scheme, the samples were magnetized in plane using an externally applied magnetic field of 0.35 T using a permanent magnet. The coherent response of the sample magnetization to the terahertz field was probed by measurements of the MOKE in polar geometry (that is, at normal incidence). Further details about the measurement geometry are provided in Supplementary Sections 1–3. In our analysis, we define a time zero looking at the electro-optical sampling data just before the first detectable oscillation of the terahertz waveform. We then kept the same time zero (that is, the same position of the delay stage) of all the MOKE scans for the respective frequency.

MOKE data normalization. The normalized MOKE curves in Fig. 2 obtained from the reflectivity data were calculated as

$$\mathrm{MOKE} = \frac{\Delta R}{2R} \times \frac{\omega/2\pi}{H_{\mathrm{THz}}} \quad (5)$$

where ΔR is the transient reflectivity change due to the THz pump, ω is the centre frequency of the terahertz pump field and H_{THz} its maximum amplitude. Error bars in the resonance amplitude were calculated by taking the standard deviation of the measurement before time zero.

Data availability

Data that support the plots within this paper and other findings of this study are available from the corresponding author upon reasonable request. Source data are provided with this paper.

References

50. Green, B. et al. High-field high-repetition-rate sources for the coherent THz control of matter. *Sci. Rep.* **6**, 22256 (2016).

Acknowledgements

We thank J. Lindner (HZDR, Dresden) for helpful discussions and Z. Wang and S. Germansky for experimental support. The research leading to this result has been partly supported by the project CALIPSOplus under grant agreement no. 730872 from the EU Framework Programme for Research and Innovation HORIZON 2020. Parts of this research were carried out at ELBE at Helmholtz-Zentrum Dresden-Rossendorf e.V., a member of the Helmholtz Association. We thank U. Lehnert and J. Teichert for assistance and the ELBE team for operating the TELBE facility. S.K., B.G. and M.G. acknowledge support from the European Cluster of Advanced Laser Light Sources (EUCALL) project, which has received funding from the European Union's Horizon 2020 Research and Innovation Programme under grant agreement no. 654220. N.A., I.I., M.G. and S.K. acknowledge support from the European Commission's Horizon 2020 research and innovation programme, under grant agreement no. DLV-737038(TRANSPIRE). K.N., D.P., N.Z.H. and S.B. acknowledge support from the European Research Council, Starting Grant 715452 MAGNETIC-SPEED-LIMIT.

Author contributions

S.B. designed the experiment. S.B. and M.G. coordinated the project. K.N., N.A., S.K., D.P., N.Z.H., B.G., J.-C.D., I.I., M.C., M.B., M.G. and S.B. performed the measurements at TELBE. K.N., N.A. and S.B. performed the data analysis. K.N., V.S., M.d'A. and C.S. performed the inertial LLG simulations. S.S.P.K.A., O.H., A.S. and K.L. fabricated and characterized the samples. K.N. and S.B. coordinated the work on the paper, with contributions from N.A., S.K., S.S.P.K.A., A.S., K.L., O.H., J.-E.W. and M.G. and discussions with all authors.

Competing interests

The authors declare no competing interests.

Additional information

Supplementary information is available for this paper at https://doi.org/10.1038/s41567-020-01040-y.

Correspondence and requests for materials should be addressed to S.B.

Reprints and permissions information is available at www.nature.com/reprints.